Journal of Sol-Gel Science and Technology (2023) 105:804–813
https://doi.org/10.1007/s10971-023-06068-z

ORIGINAL PAPER: NANO-STRUCTURED MATERIALS (PARTICLES, FIBERS, COLLOIDS, COMPOSITES, ETC.)

Bimetallic NiMo-supported Al_2O_3@TiO_2 core-shell microspheres with high hydrodeoxygenation efficiency toward syringol

The Ky Vo[1]

Received: 14 November 2022 / Accepted: 10 February 2023 / Published online: 21 February 2023

Abstract

In this work, bimetallic NiMo-supported Al_2O_3@TiO_2 core-shell microspheres were developed for the hydrodeoxygenation (HDO) of syringol. First, multi-grams of bimetallic NiMo-supported Al_2O_3 microspheres containing 20 wt% Ni and 10 wt% Mo were prepared by combining sol-gel and spray pyrolysis (NiMo@Al_2O_3). Afterwards, a TiO_2 anatase shell was decorated onto the surfaces of NiMo@Al_2O_3 microspheres by hydrolysis of titanium (IV) butoxide with the assistance of an inhibitor. The fabricated NiMo@Al_2O_3@TiO_2 spheres were characterized by XRD, FE-SEM, HR-TEM, N_2 adsorption-desorption, XPS, and H_2-TPR analyses. The results indicate that Ni and Mo species were incorporated well into the γ-Al_2O_3 microspheres, which were finely coated by a TiO_2 anatase shell layer. HDO experiments showed that the spray pyrolysis-derived bimetallic NiMo-supported catalysts effectively converted syringol with a conversion of ~100% at 270 °C for 3 h, but the hydrocarbon selectivity was still low (~40.3%). By decorating a TiO_2 layer shell onto the NiMo@Al_2O_3 microspheres, enhancing the hydrocarbon selectivity up to ~97%, which included methyl-substituted cyclohexanes (~87.7%), cyclohexane (~2%), and 1,1′-bi(cyclohexane) (~7.3%). The findings suggest that coating the NiMo@Al_2O_3 microspheres containing high catalyst contents with a hydrophobic shell resulted in a synergetic effect that improved the HDO performance.

Graphical Abstract

Hydrodeoxygenation of syringol over spray pyrolysis-derived catalysts (A) NiMo@Al_2O_3 and (B) NiMo@Al_2O_3@TiO_2 core-shell microspheres

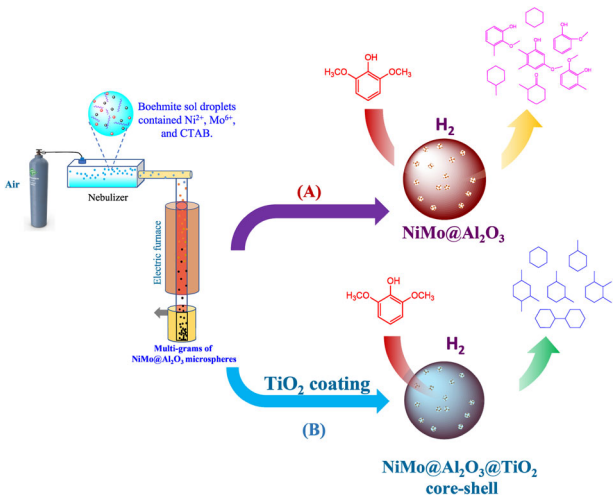

✉ The Ky Vo
votheky@iuh.edu.vn

[1] Chemical Engineering Department, Industrial university of Ho Chi Minh City, 12 Nguyen Van Bao, Go Gap, Ho Chi Minh City, Vietnam

Keywords Sol-gel · Hydrodeoxygenation · Syringol · NiMo@Al_2O_3@TiO_2 · Core-shell · Spray pyrolysis

Highlights

- NiMo@Al_2O_3 microspheres were rapidly fabricated by the spray pyrolysis.
- TiO_2 shell layer was decorated over the NiMo@Al_2O_3 microspheres.
- NiMo@Al_2O_3@TiO_2 catalyst had 100% HDO conversion toward syringol.
- NiMo@Al_2O_3@TiO_2 catalyst exhibited a good stability.

1 Introduction

Biomass-derived biofuel (bio-oil) is considered a promising alternative energy to conventional fossil fuels [1–3]. This is because the biochemical compositions of biomass (e.g., lipid and lignin) can be decomposed into low-molecular products under pyrolysis or hydrothermal liquefaction conditions [4, 5]. Nonetheless, these low-grade products usually have high acidity, viscosity, and chemical instability owing to their high contents of oxygen, nitrogen, phosphide, or sulfur, prohibiting their feasibility as vehicle fuels [6–8]. Thus, many approaches have been adopted to upgrade this low-grade biofuel, such as catalytic cracking, desulfurization, denitrogenation, or hydrodeoxygenation (HDO) [9, 10]. HDO is a promising strategy to upgrade bio-oil, by which a catalyst will eliminate oxygen in biomass-derived molecules in the presence of hydrogen [11, 12]. After treatment, the hydrodeoxygenated products achieve more hydrogen and less oxygen, leading to a higher heating value and chemical stability.

An efficient catalyst for HDO performance acquires high reactivity to effectively cleavage C-O bonds of biomass-derived molecules to achieve high hydrodeoxygenation conversion and high hydrocarbon selectivity. In addition, the catalysts must retain their reactivity for the long term to meet the realistic application requirement. However, research has indicated that catalysts' reactivity usually diminishes for several reasons. Among them, the presence of water in the reaction mixture can cause catalyst deactivation owing to the water adsorption and the formation of hydroxyl species [6, 13]. Thus, preparing a catalyst with a high water-resistance capability to achieve a good HDO performance is highly desired. This requires a good design of the compositions and structures of heterogeneous catalysts.

Many types of catalysts have been studied for HDO processes, mainly categorized as sulfide [14, 15], phosphide [16], noble metal-supported [7], and transition metal-supported catalysts [17, 18]. The sulfide catalysts require pre-treatment with H_2S, and they can release sulfur into the bio-oil as a contaminant during the HDO process, consequently reducing fuel quality. Meanwhile, the industry's use of noble metal-containing catalysts is still limited because of their prohibitive costs. Contrarily, transition metals such as Ni, Mo, and Co are relatively affordable and clean, making them more attractive materials [18, 19]. Notably, bimetallic catalyst systems of transition metals, such as NiMo, NiCo, or CoMo, are more reactive than the monometallic systems because of the significant synergy between two catalysts [17, 20–23], rendering them the most desirable candidates for hydrodeoxygenation. For instance, NiCo/γ-Al_2O_3 catalyst reportedly exhibited better guaiacol conversion than monometallic Ni or Co-supported catalysts [24]. Recently, Adilina et al. [25] synthesized a clay-supported NiMo catalyst, which showed a relatively good HDO performance toward guaiacol. Nevertheless, these catalysts were insufficient to cleavage the O–C_{aryl} bonds of the lignin-derived molecules, resulting in low hydrocarbon selectivity.

In this work, we developed NiMo@γ-Al_2O_3@TiO_2 core-shell microspheres and applied them for hydrodeoxygenation. The advantage is that high catalyst contents of Ni (20 wt%) and Mo (10 wt%) were finely incorporated into the γ-Al_2O_3 support through the combination of sol-gel and spray pyrolysis, which is a rapid and scalable approach (Fig. 1). These microspheres were then decorated with a TiO_2 shell layer, expecting to increase the catalysts' durability because of their hydrophobic nature. In the present work, syringol (2, 6-dimethoxylphenol), one of the lignin-derived model compounds [4], was subjected to hydrodeoxygenation using the prepared NiMo-supported Al_2O_3@TiO_2 core-shell catalyst. As a result, it was realized that syringol was effectively hydro deoxygenated, giving a high conversion and hydrocarbon selectivity. In addition, the prepared NiMo@Al_2O_3@TiO_2 catalyst exhibited good renewability, making it a promising catalyst for upgrading biofuel.

2 Experimental

2.1 Synthesis of NiMo@Al_2O_3 micmicrosphere

Multi-grams of bimetallic NiMo-supported γ-Al_2O_3 mesoporous microspheres were rapidly produced by the spray pyrolysis approach according to our previous work [18]. Briefly, a sol solution γ-AlOOH (0.3 M) was first prepared by the hydrolysis of aluminium-tri-sec butoxide ($Al(OC_4H_9)_3$,

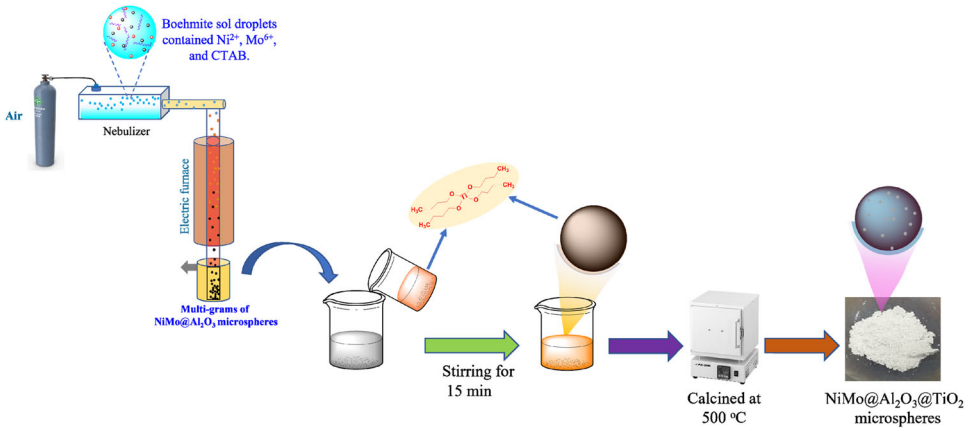

Fig. 1 The schematic diagram for the preparation of spray pyrolysis-derived $NiMo@Al_2O_3@TiO_2$ core-shell microspheres

Aldrich, 99%). Next, the precursor solution for the spray pyrolysis was prepared by dissolving $Ni(NO_3)_2.6H_2O$ (Aldrich, 97%), $(NH_4)_6Mo_7O_{24}.4H_2O$ (Aldrich, 97%), and cetyltrimethylammonium bromide (CTAB, Aldrich, 97%) into 400 ml sol with a constant stirring. Herein, CTAB acts as a surfactant that enhances the metal salt dispersion in the sol solution, and the metal/CTAB molar ratio was 0.5. The weight percentage of Ni and Mo of the catalyst was fixed at 20 and 10 wt%, respectively, which reportedly created the maximum synergetic effect of the catalyst [17]. Afterwards, the solution was nebulized to sol droplets, being brought into a quartz reactor preheated at 650 °C by airflow. The resultant powder was then calcined at 500 °C for 4 h in the air to yield the final product, which is labelled as $NiMo@Al_2O_3$.

2.2 Synthesis of $NiMo@Al_2O_3@TiO_2$ core-shell

A bimetallic NiMo-supported γ-Al_2O_3 covered TiO_2 layer was prepared according to our previous work with a slight modification [6]. First, solution X was prepared by dispersing 0.75 g spray pyrolysis-derived $NiMo@Al_2O_3$ microspheres into a solution containing ethanol (70 ml) and triethanolamine (1 ml) under vigorous stirring conditions. Solution Y was separately prepared by dissolving titanium (IV) butoxide (6 ml) in 10 ml ethanol. Then, solution Y was dropped slowly into solution X and stirred for 30 min. The solid was recovered by centrifugation and dried at 115 °C for 6 h. The obtained product was then calcined at 500 °C for 4 h in the air. Finally, the product was subjected to a reduction at 700 °C for 3 h using a gas flow of 15%H_2/Ar in a fixed-bed reactor to obtain the final product $NiMo@Al_2O_3@TiO_2$.

2.3 Characterizations

The prepared materials' morphology was obtained by high-resolution FE-SEM (HR-FESEM, Carl Zeiss STM, Germany) and TEM (Talos F200X). The textural properties of the prepared catalysts were analyzed by nitrogen sorption at 77 K using an N_2 porosimeter (BELSORP-max, BEL, Osaka, Japan). Before analyzing, all samples were degassed at 150 °C for 8 h under vacuum conditions. The specific surface area of the sample was measured using the multi-point Brunauer–Emmet–Teller method, and the pore size distribution was obtained by applying the Barrett–Joyner–Halender (BJH) method. The crystalline structures of the catalysts were analyzed by utilizing a powder X-ray diffractometry (XRD) with a Cu Kα radiation source (Rigaku, Tokyo, Japan). The chemical states of Mo and Ni elements were examined by X-ray photoelectron spectrometry (XPS; K-Alpha, Thermo Fisher Scientific, Waltham, MA, USA). Before analysis, the reduced catalyst was passivated in a gas flow of 1% O_2/Ar for 3 h at room temperature. Binding energy was corrected based on the binding energy value of the adventitious carbon C1s (284.6 eV).

The H_2 temperature-programmed reduction (H_2-TPR) was performed using the fixed-bed reactor. First, 0.2 g calcined catalyst was loaded into the reactor and treated at 150 °C for 1 h under Ar flow (60 ml/min) to remove physically adsorbed impurities. Then, the reduction was carried out using a gas flow of 20%H_2/Ar, and the reduction temperature was increased up to 900 °C at a heating rate of 3 °C/min. The downstream H_2 was analyzed by a gas chromatograph (6500GC, Y.L. Instrument, Korea) equipped with a thermal conductivity detector.

2.4 Hydrodeoxygenation of syringol

In this work, syringol, a methoxy-substituted phenol, one of the lignin-derived compounds, was utilized as a bio-oil model compound. The hydrodeoxygenation of syringol was carried out using a high-pressure autoclave reactor. First, 50 ml of decane and 0.1 g of syringol were loaded into the reactor. Next, a 0.3 g catalyst ($NiMo@Al_2O_3$ and $NiMo@Al_2O_3@TiO_2$) was added to the mixture. After

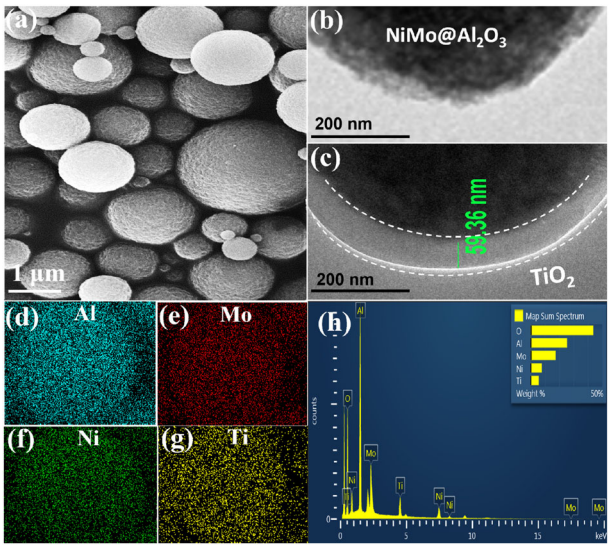

Fig. 2 **a** HRFE-SEM image of NiMo@Al_2O_3 and HR-TEM image of **b** NiMo@Al_2O_3 and **c** NiMo@Al_2O_3@TiO_2; **d–h** EDX elemental maps of Al, Mo, Ni, and Ti of the NiMo@Al_2O_3@TiO_2 microsphere

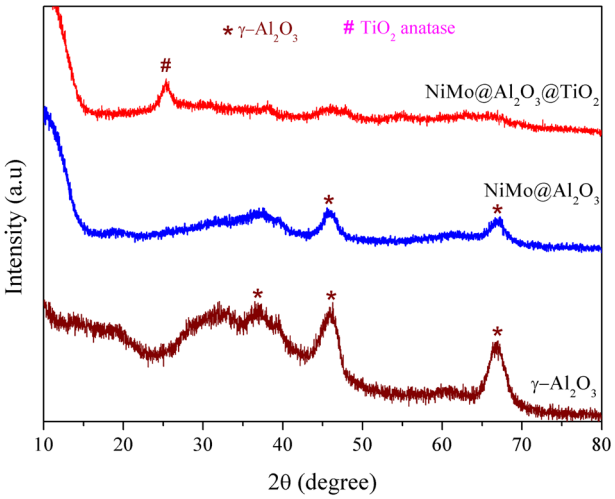

Fig. 3 XRD patterns of the prepared γ-Al_2O_3, NiMo@Al_2O_3, and NiMo@Al_2O_3@TiO_2

being sealed, the air inside the reactor was replaced by H_2 (4 MPa). Afterwards, the reactor was heated to the designed temperature under stirring conditions and kept for 3 h. The reactor was then naturally cooled to room temperature. The liquid product was obtained by filtering and then analyzed using Gas chromatography-Mass spectroscopy (GC-MS; Agilent 7890 A, USA). The HDO conversion was calculated from the converted syringol/initial syringol ratio, while the product selectivities were obtained based on the moles of each component in the downstream product.

For the cyclic experiments, the catalyst was dried at 120 °C and vacuumed (10^{-2} kPa) for two hours before being used for the next run. Other reaction conditions were maintained for all experiments.

3 Results and discussion

3.1 Characterization

The morphology of the prepared samples was examined through SEM and TEM measurements, as presented in Fig. 2. The SEM image of spray pyrolysis-derived NiMo@Al_2O_3 shows microspheres with particle sizes of 0.3~2.0 µm [Fig. 2a]. The TEM image demonstrates a TiO_2 shell layer with a thickness of ~59 nm decorated over the microsphere NiMo@Al_2O_3 [Fig. 1b, c]. In addition, EDX elemental maps analyses confirmed the presence of Ni and Mo dopants, which were finely dispersed throughout the spheres [Fig. 1d–h]. Figure 3 shows crystallography analyses of the prepared γ-Al_2O_3, NiMo@Al_2O_3, and NiMo@Al_2O_3@TiO_2 catalyst. As demonstrated, the XRD pattern of the bare Al_2O_3 showed diffraction peaks at $2\theta = 37.6°$, 46.0°, and 66.7°, which are the characteristics of the γ-Al_2O_3 phase. There is no trace of metal dopants witnessed on the XRD pattern of the bimetallic NiMo-supported Al_2O_3 samples. This suggests that these metal species were finely incorporated into the support γ-Al_2O_3 and could be beyond the XRD detection limitation. The same phenomenon was previously reported for spray pyrolysis-derived materials [18, 26, 27]. It is notable that the NiMo@Al_2O_3@TiO_2 catalyst's peak intensities were slightly diminished owing to the newly formed TiO_2 shell layer.

The catalyst's reduction behavior and its elements' valence states were analyzed, and the results are illustrated in Fig. 4. Figure 4a reveals the H_2-TPR profile of the calcined NiMo@Al_2O_3@TiO_2 catalysts. As illustrated, the low-temperature peak at around 390 °C is attributed to the reduction of Mo^{6+} to Mo^{4+} [18]; the broader peak ranged 450 ~ 810 °C is ascribed to the reduction of Mo^{4+} and Ni^{2+} to metallic Mo^0 and Ni^0, respectively [17, 18]. Herein, it should be mentioned that the reduction of metal oxide species of the NiMo-supported catalyst is much more facilitated than monometallic Mo or Ni-supported catalysts owing to the synergetic effect of the bimetallic system [18]. We further examined the valence states of Ni and Mo of the synthesized catalysts using XPS analyses, and the results are presented in Fig. 4b, c. As revealed in Fig. 4b, the O 1 s XPS spectrum of the calcined NiMo@γ-Al_2O_3@TiO_2 shows two peaks at around 530.4 eV and 532.5 eV. The low binding energy peak is ascribed to M-O bonds (M: Al, Ti, Ni, and Mo), while the higher binding energy peak is attributed to the H–O bonds of the adsorbed water molecules [28]. For the reduced sample, the high energy peak of O disappeared on the O 1 s XPS spectrum due to the

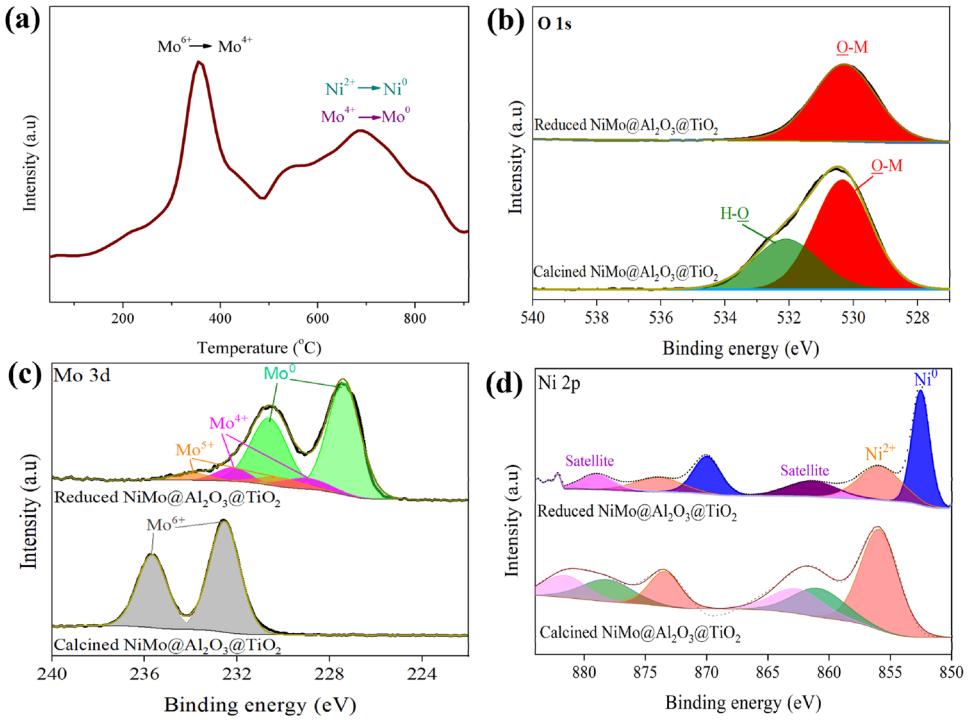

Fig. 4 **a** H_2-TPR profile and the high-resolution XPS spectrum of **b** O 1 s, **c** Mo 3d, and **d** Ni 2p of NiMo@Al_2O_3@TiO_2

elimination of the adsorbed water during the reduction process. Moreover, the peak of the M–O bonds shows a decrease in intensity, which could result from the reduction of molybdenum and nickel oxides. The high-resolution XPS spectrum of Mo in the calcined NiMo@Al_2O_3@TiO_2 shows the binding energy peak of 232.7 eV (Mo $3d_{5/2}$) and 235.9 eV (Mo $3d_{3/2}$), which are characteristics of Mo^{6+} [29]. After reduction, the Mo 3d spectrum shows the coexistence of Mo^{5+} (231.5 and 234.6 eV), Mo^{4+} (229.3 and 232.4 eV), and Mo^0 (227.9 and 230.8 eV) [6, 28] [Fig. 4c]. Accordingly, the percentage of Mo^0, Mo^{4+}, and Mo^{5+} was approximately 78, 13, and 9%, respectively. Concerning the nickel, the high-resolution XPS spectrum of Ni 2p in the calcined catalyst exhibits the energy peak of 857.2 eV (Ni $2p_{3/2}$) and 874.7 eV (Ni $2p_{1/2}$) along with a broad shake-up satellite, which are the characteristics of Ni^{2+} [24]. In addition, the Ni 2p XPS spectrum of the reduced NiMo@γ-Al_2O_3@TiO_2 sample indicates that Ni^{2+} was reduced to metallic Ni^0, which is confirmed via the binding energy peak at 852.3 and 870.1 eV [24] [Fig. 4d]. The findings indicate that the reduced NiMo@Al_2O_3@TiO_2 microspheres contained high amounts of Mo^0 and Ni^0, which are beneficial for the hydrodeoxygenation performance.

N_2 sorption curves and pore size distributions of the fabricated samples were demonstrated in Fig. 5a and Fig. 5b, respectively. Table 1 lists the samples' calculated BET surface area and pore volume. As shown in Table 1, the spray pyrolysis-derived NiMo-supported Al_2O_3 microspheres had BET surface area and pore volume of ~280 m^2/g and ~0.28 cm^3/g, respectively. The synthesized TiO_2-coated NiMo@Al_2O_3 sample had surface area and pore volume of 220 m^2/g and 0.23 cm^3/g, respectively, showing a slight decrease in porosity compared to the pristine NiMo@Al_2O_3 samples owing to the newly decorated TiO_2 shell layer.

3.2 Hydrodeoxygenation of syringol

Figure 6a–c show the GC-MS analysis results of the hydrodeoxygenation of syringol using the fabricated catalysts compared with the catalyst blank experiment. As shown, no trace of products was observed on the GC/MS spectrum for the catalyst blank experiment. Nonetheless, the GC-MS spectra for the downstream products obtained for the catalytic experiments exhibit many substances, suggesting syringol was converted over the NiMo@Al_2O_3 and NiMo@Al_2O_3@TiO_2 catalysts. Table 2 lists the obtained products with a quality higher than 90%. The obtained results evidenced that spray pyrolysis-derived bimetallic NiMo-supported Al_2O_3 effectively converted syringol, giving a high HDO conversion of 100% after a holding time of 3 h. However, it should be noted that there is a significant difference in the product distribution and selectivity achieved for the prepared catalysts. As revealed in Table 2, the catalytic hydrodeoxygenation of syringol over the pristine NiMo@Al_2O_3 sample produced a wide product distribution, giving a selectivity of ~56.4 and ~40.3% for oxygenated- and deoxygenated products, respectively. Contrarily, the NiMo@Al_2O_3@TiO_2 core-shell converted syringol to methyl-substituted cyclohexanes (~87.7%),

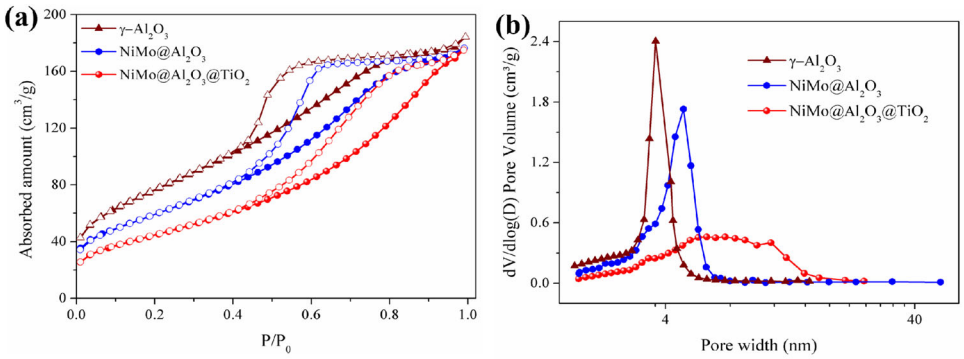

Fig. 5 Textural properties of the prepared samples: **a** N_2 adsorption-desorption curves and **b** Pore size distributions

Table 1 BET surface area and pore volume of the prepared materials

Sample	BET surface area, m^2/g	Total pore volume, cm^3/g	Mean pore diameter, nm
γ-Al_2O_3	310	0.30	2.8
NiMo@Al_2O_3	280	0.28	3.1
NiMo@Al_2O_3@TiO_2	220	0.23	4.4

cyclohexane (~2.0%), and 1,1′-bi(cyclohexane) (~7.3%), giving a hydrocarbon selectivity of up to ~97%. These results evidenced that the NiMo@Al_2O_3@TiO_2 core-shell was much more selective for deoxygenated products. This can be explained by the fact that the decorated TiO_2 anatase shell could protect the metallic catalysts owing to its hydrophobic nature. Indeed, the active sites of Ni^0 and Mo^0 might rapidly lose their reactivities due to water adsorption and the formation of hydroxyl species (-M-OH). Therefore, the TiO_2-coated NiMo@Al_2O_3 microspheres improved the HDO performance toward the investigated lignin-derived model compared to the uncoated counterpart. Moreover, the decorated TiO_2 could generate defects such as oxygen vacancy, enhancing the accumulation of the O-containing compounds onto the catalyst [30, 31]. The findings indicated that coating the NiMo@Al_2O_3 microspheres containing high catalyst contents with a hydrophobic shell resulted in a synergetic effect that enhanced the catalytic performance.

3.3 Hydrodeoxygenation mechanism

As syringol is a methoxy-substituted phenol, its conversion could include a few reaction mechanisms, such as demethoxylation (DEMET), demethylation (DEMELA), methylation (MELA), hydrogenation (HYD), hydrodeoxygenation (HDO), and isomerization [21, 32, 33]. As listed in Table 2, the major products were ring-hydrogenated species, such as dimethylcyclohexane, trimethylcyclohexane, and bicyclohexyl. Besides, methyl- and methoxy-substituted benzene and phenol were also witnessed for the NiMo@Al_2O_3 catalyst.

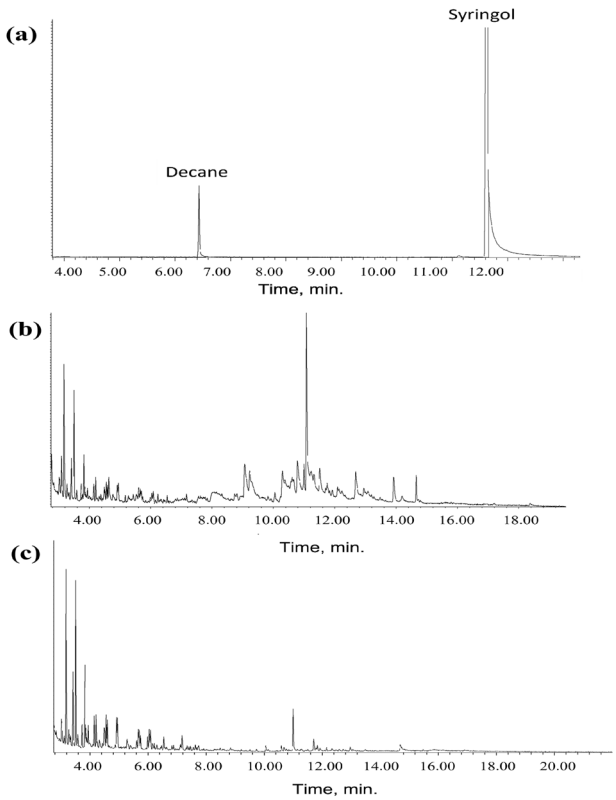

Fig. 6 GC-MS spectrum of the products for **a** catalyst blank, **b** NiMo@Al_2O_3, and **c** NiMo@Al_2O_3@TiO_2

Therefore, based on the identified products, several reaction pathways were proposed to involve the conversion of syringol, as demonstrated in Fig. 7. The first reaction pathway consists of the demethoxylation of syringol to 2-methoxyl phenol (guaiacol, (9)) or 3-methoxyl phenol (*m*-guaiacol, (13)). Next, *m*-guaiacol could be demethoxylated to phenol and benzene. Benzene could dimerize to produce 1,1′-biphenyl, followed by hydrogenation to bicyclohexyl. Besides, phenol could also be subjected to methylation to produce 2,4,6-trimethylphenol, which was converted to 1,3,5-trimethylcyclohexane (18). Moreover, *m*-guaiacol could be converted to 5-methoxy-2,3-dimethylphenol (17) through

Table 2 Product distribution obtained for the HDO of syringol utilizing the prepared $NiMo@Al_2O_3$ and $NiMo@Al_2O_3@TiO_2$ catalysts

No.	$NiMo@Al_2O_3$		$NiMo@Al_2O_3@TiO_2$	
	Compounds	Selectivity,%	Compounds	Selectivity,%
1	methylcyclohexene	4.0	methylcyclohexane	9.4
2	1,3-dimethylcyclohexane	9.7	1,3-dimethylcyclohexane	10.8
3	1,2-dimethylcyclohexane	5.8	1,2-dimethylcyclohexane	14.6
4	1,4-dimethylcyclohexane	5.6	1,4-dimethylcyclohexane	12.3
5	1,2,4-trimethylcyclohexane	4.5	1,2,4-trimethylcyclohexae	15.3
6	1,2,3-trimethylcyclohexane	7.2	1,2,3-trimethylcyclohexane	13.2
7	2-methylcyclohexanone	3.5	–	–
9	2-methoxyphenol	7.2	–	–
10	1,3-dimethoxybenzene	6.4	–	–
11	2-methoxy-3-methylphenol	7.2	–	–
12	2,6-dimethoxytoluene	4.4	–	–
13	3-methoxyphenol	4.5	–	–
14	2-methoxy-6-methylphenol	5.1	–	–
15	1,2,3-trimethoxybenzene	14.2	–	–
16	1,2-dimethoxybenzene	2.6	–	–
17	5-methoxy-2,3-dimethylphenol	4.8	–	–
18	–	–	1,3,5-trimethylcyclohexane	6.2
19	–	–	1,2,3,5-tetramethylcyclohexane	2.3
20	–	–	1,1,2,3-tetramethylcyclohexane	3.6
21	Cyclohexane	3.4	Cyclohexane	2.0
22	–	–	1,1′-bi(cyclohexane)	7.4
	Total	**96.7**		**97.1**

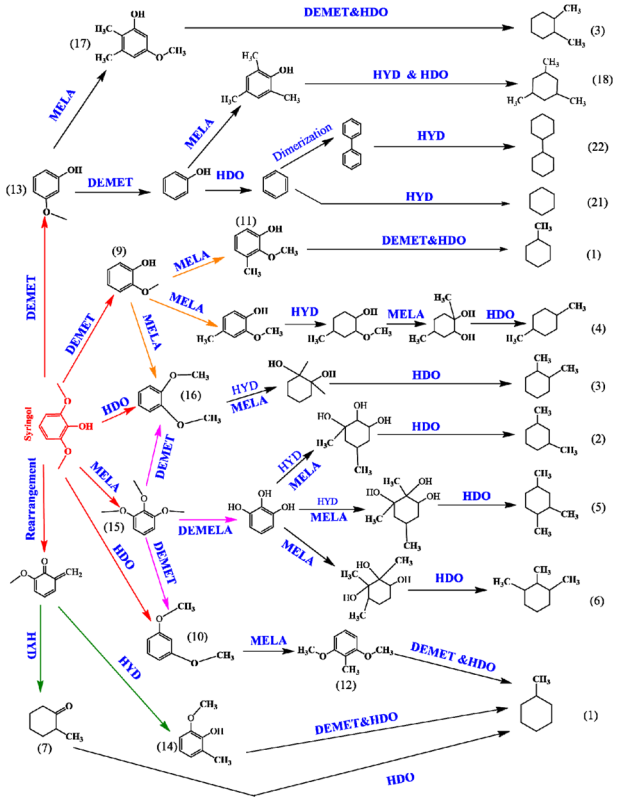

Fig. 7 The proposed mechanism for the HDO conversion of syringol utilizing the prepared $NiMo@Al_2O_3@TiO_2$ core-shell microspheres (The compounds correspond to those from Table 2)

methylation, followed by creating 1,2-dimethyl cyclohexane (3) via the DEMET and HDO processes. Guaiacol could be methylated to 2-methoxy-3-methylphenol (11) and 2-methoxy-4-methylphenol, which was eventually hydrodeoxygenated to methylcyclohexane (1) and 1,4-dimethyl cyclohexane (4), respectively. The second reaction pathway is that syringol could be partially hydrodeoxygenated to 1,2-dimethoxybenzene (16) or 1,3-dimethoxybenzene (10). These intermediates were converted to methylcyclohexane (1) and 1,2-dimethylcyclohexane (3) through hydrodeoxygenation and demethylation. The third reaction pathway directly converts syringol to 1,2,3-trimethoxybenzene (15) via methylation. Then, trimethoxybenzene could be converted to 1,2 -dimethoxybenzene (16) and 1,3-dimethoxybenzene (10) due to the demethylation. In addition, trimethoxylbenzene also could be converted to 2,3-dimethoxy-5-methylphenol or 2,3-dimethoxy-6-methylphenol via methylation, which conventionally generated 1,2,4-trimethylcyclohexane (5) or 1,2,3-trimethylcyclohexane (6) via the MELA and HDO mechanisms. The fourth reaction pathway could involve the rearrangement of syringol to form 2-methoxy-6-methylenecyclohexa-2,4-dien-1-one, which was then converted to 2-methoxy-6-methylphenol (14) due to the HYD and DEMET reactions. These products were finally hydrogenated and hydrodeoxygenated to methylcyclohexane (1). It is noticeable that methyl-substituted cyclohexane such as 1,2,3,5-tetramethylcyclohexane (19) and 1,1,2,3-tetramethylcyclohexane (20) are only observed in the product

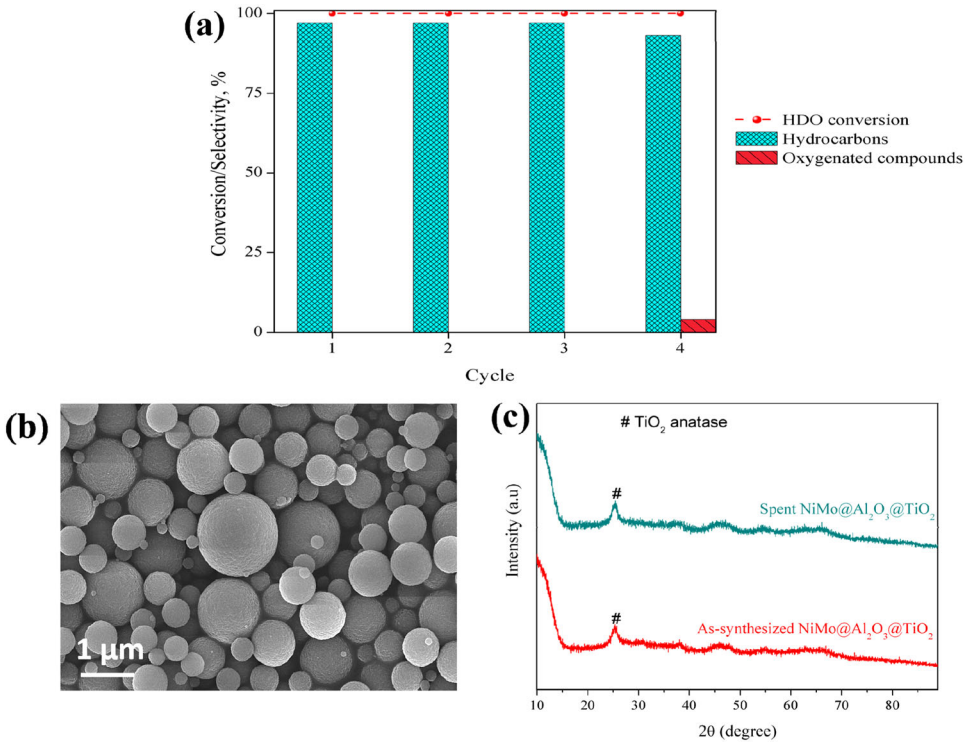

Fig. 8 **a** HDO conversion and product selectivity after four cycles, **b** SEM image, and **c** XRD pattern of the spent $NiMo@Al_2O_3@TiO_2$ catalyst

stream for the $NiMo@Al_2O_3@TiO_2$ core-shell catalyst. These suggest that the TiO_2-coated $NiMo@Al_2O_3$ microspheres could further facilitate isomerization and methylation due to their improved catalytic activity and stability.

3.4 Reusability tests

Successive cyclic experiments were performed to further evaluate the $NiMo@Al_2O_3@TiO_2$ core-shell catalyst's reactivities. After each run, the catalyst was recovered and dried at 120 °C under vacuum conditions for two hours before being used as a regenerated catalyst. Figure 8a shows the HDO conversion of syringol and product selectivities after four cyclic experiments. As depicted, the HDO conversion of syringol remained 100% after four runs. Moreover, the hydrocarbon selectivity retained approximately 97% after three cycles before slightly dropping to ~94% after the fourth run. The recycled catalyst's morphology and crystallography were examined, and the results are presented in Fig. 8b and c, respectively. As depicted in Fig. 8b, $NiMo@Al_2O_3@TiO_2$ catalyst' morphology was unchanged after several runs. Furthermore, the recycled sample's XRD pattern remains the same as the as-prepared catalyst without a trace of exposed metals. That is to say, the active metal catalysts were preserved well within the host matrix. The results evidenced that the fabricated $NiMo@Al_2O_3@TiO_2$ had good renewability and durability.

4 Conclusions

Mesoporous core-shell microspheres $NiMo@Al_2O_3@TiO_2$ contained 20 wt% Ni and 10 wt% Mo were prepared by combining spray pyrolysis and hydrolysis. The prepared $NiMo@Al_2O_3@TiO_2$ had a specific surface area of 220 m^2/g and a pore volume of 0.23 cm^3/g, respectively. The synthesized $NiMo@Al_2O_3@TiO_2$ core-shell microspheres exhibited an outperforming hydrodeoxygenation toward syringol with a conversion of ~100% at 270 °C for 3 h. Notably, by constructing a hydrophobic TiO_2 shell over the $NiMo@Al_2O_3$ microsphere, their catalytic activities remarkably enhanced, giving a higher hydrocarbon selectivity (~97%) than the pristine $NiMo@Al_2O_3$ catalyst (~40.3%). The conversion of syringol catalyzed by $NiMo@Al_2O_3@TiO_2$ catalyst produced methyl-substituted cyclohexane as the predominant product (total selectivity ~87.7%). Furthermore, the synthesized $NiMo@Al_2O_3@TiO_2$ core-shell microspheres retained high syringol conversion and hydrocarbon selectivity over four runs. The findings suggest that the spray pyrolysis-derived $NiMo@Al_2O_3@TiO_2$ core-shell microsphere is a promising catalyst candidate for hydrodeoxygenation performance.

Data availability

The data is true and reliable.

Acknowledgements This work is supported by the Industrial University of Ho Chi Minh City. The author also thanks Professor Jinsoo Kim at Chemical Engineering Department for his support.

Author contributions TKV: Conceptualization, investigation, formal analysis, writing manuscript, visualization, editing & reviewing.

Funding This research is funded by Vietnam National Foundation for Science and Technology Development (NAFOSTED) under grant number 104.05-2020.32. This work is supported by the Industrial University of Ho Chi Minh City.

Compliance with ethical standards

Conflict of interest The author declares no competing interests.

Ethical approval Not applicable.

Consent to participate All authors agree to participate in the editing of the paper.

Consent to publish All authors agree to publish this manuscript in your journal.

References

1. Chen H, Xia A, Zhu X, Huang Y, Zhu X, Liao Q (2022) Hydrothermal hydrolysis of algal biomass for biofuels production: A review. Bioresour Technol 344:126213. https://doi.org/10.1016/j.biortech.2021.126213
2. Su G, Ong HC, Gan YY, Chen W-H, Chong CT, Ok YS (2022) Co-pyrolysis of microalgae and other biomass wastes for the production of high-quality bio-oil: Progress and prospective. Bioresour Technol 344:126096. https://doi.org/10.1016/j.biortech.2021.126096
3. Ashokkumar V, Venkatkarthick R, Jayashree S, Chuetor S, Dharmaraj S, Kumar G, Chen W-H, Ngamcharussrivichai C (2022) Recent advances in lignocellulosic biomass for biofuels and value-added bioproducts—A critical review. Bioresour Technol 344:126195. https://doi.org/10.1016/j.biortech.2021.126195
4. Vo TK, Cho J-S, Kim S-S, Ko J-H, Kim J (2017) Genetically engineered hybrid poplars for the pyrolytic production of bio-oil: Pyrolysis characteristics and kinetics. Energy Convers Manag 153:48–59. https://doi.org/10.1016/j.enconman.2017.10.001
5. Vo TK, Kim S-S, Kim J (2022) Pyrolysis characteristics and quantitative kinetic model of microalgae Tetralselmis sp. Korean J Chem Eng. https://doi.org/10.1007/s11814-022-1064-9
6. Vo TK, Quang DT, Kim J (2022) Spray pyrolysis-derived MoO_3@Al_2O_3@TiO_2 core-shell structures with enhanced hydrodeoxygenation performance. Catal Commun. 169:106478. https://doi.org/10.1016/j.catcom.2022.106478
7. Martinez-Klimov M, Mäki-Arvela P, Çiftçi A, Kumar N, Eränen K, Peurla M, Hensen EJM, Murzin DY (2022) Bifunctional Pt–Re Catalysts in Hydrodeoxygenation of Isoeugenol as a model compound for renewable jet fuel production. ACS Eng Au. https://doi.org/10.1021/acsengineeringau.2c00015
8. Shi Y, Xing E, Wu K, Wang J, Yang M, Wu Y (2017) Recent progress on upgrading of bio-oil to hydrocarbons over metal/zeolite bifunctional catalysts. Catal Sci Technol 7(12):2385–2415. https://doi.org/10.1039/C7CY00574A
9. Baloch HA, Nizamuddin S, Siddiqui MTH, Riaz S, Jatoi AS, Dumbre DK, Mubarak NM, Srinivasan MP, Griffin GJ (2018) Recent advances in production and upgrading of bio-oil from biomass: A critical overview. J Environ Chem Eng 6(4):5101–5118. https://doi.org/10.1016/j.jece.2018.07.050
10. Srifa A, Chaiwat W, Pitakjakpipop P, Anutrasakda W, Faungnawakij K (2019) Chapter 6—Advances in bio-oil production and upgrading technologies. In: Rai M, Ingle AP (eds) Sustainable Bioenergy. Elsevier, pp 167–198. https://doi.org/10.1016/B978-0-12-817654-2.00006-X
11. Prabhudesai VS, Gurrala L, Vinu R (2022) Catalytic hydrodeoxygenation of lignin-derived oxygenates: catalysis, mechanism, and effect of process conditions. Energy Fuels 36(3):1155–1188. https://doi.org/10.1021/acs.energyfuels.1c02640
12. Kim S, Kwon EE, Kim YT, Jung S, Kim HJ, Huber GW, Lee J (2019) Recent advances in hydrodeoxygenation of biomass-derived oxygenates over heterogeneous catalysts. Green Chem 21(14):3715–3743. https://doi.org/10.1039/C9GC01210A
13. Song H, Gong J, Song H-L, Li F, Zhang J, Chen Y-G (2016) Preparation of core-shell structured Ni2P/Al_2O_3@TiO_2 and its hydrodeoxygenation performance for benzofuran. Catal Commun 85:1–4. https://doi.org/10.1016/j.catcom.2016.07.005
14. Romero CMC, Thybaut JW, Marin GB (2008) Naphthalene hydrogenation over a NiMo/γ-Al_2O_3 catalyst: Experimental study and kinetic modelling. Catal Today 130(1):231–242. https://doi.org/10.1016/j.cattod.2007.06.074
15. Bui VN, Laurenti D, Afanasiev P, Geantet C (2011) Hydrodeoxygenation of guaiacol with CoMo catalysts. Part I: Promoting effect of cobalt on HDO selectivity and activity. Appl Catal B 101(3):239–245. https://doi.org/10.1016/j.apcatb.2010.10.025
16. Yun G-N, Ahn S-J, Takagaki A, Kikuchi R, Oyama ST (2017) Hydrodeoxygenation of γ-valerolactone on bimetallic NiMo phosphide catalysts. J Catal 353:141–151. https://doi.org/10.1016/j.jcat.2017.07.006
17. Phan D-P, Vo TK, Le VN, Kim J, Lee EY (2020) Spray pyrolysis synthesis of bimetallic NiMo/Al_2O_3–TiO_2 catalyst for hydrodeoxygenation of guaiacol: Effects of bimetallic composition and reduction temperature. J Ind Eng Chem 83:351–358. https://doi.org/10.1016/j.jiec.2019.12.008
18. Vo TK, Kim W-S, Kim S-S, Yoo KS, Kim J (2018) Facile synthesis of Mo/Al_2O_3–TiO_2 catalysts using spray pyrolysis and their catalytic activity for hydrodeoxygenation. Energy Convers Manag 158:92–102. https://doi.org/10.1016/j.enconman.2017.12.049
19. Zhang Z, Shen C, Sun K, Jia X, Ye J, Liu C-J (2022) Advances in studies of the structural effects of supported Ni catalysts for CO_2 hydrogenation: from nanoparticle to single atom catalyst. J Mater Chem A 10(11):5792–5812. https://doi.org/10.1039/D1TA09914K
20. López-Cruz C, Guzman J, Cao G, Martínez C, Corma A (2021) Modifying the catalytic properties of hydrotreating NiMo–S phases by changing the electrodonor capacity of the support. Catal Today 382:130–141. https://doi.org/10.1016/j.cattod.2021.08.002
21. Mora-Vergara ID, Hernández Moscoso L, Gaigneaux EM, Giraldo SA, Baldovino-Medrano VG (2018) Hydrodeoxygenation of guaiacol using NiMo and CoMo catalysts supported on alumina modified with potassium. Catal Today 302:125–135. https://doi.org/10.1016/j.cattod.2017.07.015
22. Kaluža L, Kubička D (2017) The comparison of Co, Ni, Mo, CoMo, and NiMo sulfided catalysts in rapeseed oil hydrodeoxygenation. React Kinet Mech Catal 122(1):333–341. https://doi.org/10.1007/s11144-017-1247-2
23. Patil RB, House SD, Mantri A, Yang JC, McKone JR (2020) Direct observation of Ni–Mo bimetallic catalyst formation via

thermal reduction of nickel molybdate nanorods. ACS Catal 10(18):10390–10398. https://doi.org/10.1021/acscatal.0c02264
24. Zhou M, Ye J, Liu P, Xu J, Jiang J (2017) Water-assisted selective hydrodeoxygenation of guaiacol to cyclohexanol over supported Ni and Co bimetallic catalysts. ACS Sustain Chem Eng 5(10):8824–8835. https://doi.org/10.1021/acssuschemeng.7b01615
25. Adilina IB, Rinaldi N, Simanungkalit SP, Aulia F, Oemry F, Stenning GBG, Silverwood IP, Parker SF (2019) Hydrodeoxygenation of Guaiacol as a Bio-oil model compound over pillared clay-supported Nickel–Molybdenum catalysts. J Phys Chem C 123(35):21429–21439. https://doi.org/10.1021/acs.jpcc.9b01890
26. Vo TK (2022) Spray pyrolysis synthesis and UV-driven photocatalytic activity of mesoporous Al_2O_3@TiO_2 microspheres. Environ Sci Pollut Res. https://doi.org/10.1007/s11356-022-18865-0
27. Ly HV, Im K, Go Y, Galiwango E, Kim S-S, Kim J, Choi JH, Woo HC (2016) Spray pyrolysis synthesis of γ-Al_2O_3 supported metal and metal phosphide catalysts and their activity in the hydrodeoxygenation of a bio-oil model compound. Energy Convers Manag 127:545–553. https://doi.org/10.1016/j.enconman.2016.09.020
28. Su D, Zhang X, Wu A, Yan H, Liu Z, Wang L, Tian C, Fu H (2019) CoO-Mo2N hollow heterostructure for high-efficiency electrocatalytic hydrogen evolution reaction. NPG Asia Mater 11(1):78. https://doi.org/10.1038/s41427-019-0177-z
29. Ji W, Shen R, Yang R, Yu G, Guo X, Peng L, Ding W (2014) Partially nitrided molybdenum trioxide with promoted performance as an anode material for lithium-ion batteries. J Mater Chem A 2(3):699–704. https://doi.org/10.1039/C3TA13708B
30. Vo TK (2022) Mo-modified TiO_2 mesoporous microspheres prepared by spray pyrolysis for adsorption-photocatalytic water remediation. J Sol-Gel Sci Technol 103(3):853–864. https://doi.org/10.1007/s10971-022-05902-0
31. Shayegan Z, Lee C-S, Haghighat F (2018) TiO_2 photocatalyst for removal of volatile organic compounds in gas phase—A review. Chem Eng J 334:2408–2439. https://doi.org/10.1016/j.cej.2017.09.153
32. Asmadi M, Kawamoto H, Saka S (2011) Thermal reactions of guaiacol and syringol as lignin model aromatic nuclei. J Anal Appl Pyrolysis 92(1):88–98. https://doi.org/10.1016/j.jaap.2011.04.011
33. Feliczak-Guzik A, Szczyglewska P, Jaroniec M, Nowak I (2020) Ruthenium-containing SBA-12 catalysts for anisole hydrodeoxygenation. Catal Today 354:67–76. https://doi.org/10.1016/j.cattod.2020.03.006